Computer Assisted Mechanics and Engineering Sciences, 15: 353–368, 2008.


# The Trefftz finite elements modelling crack propagation

Henryk Sanecki, Andrzej P. Zieliński
*Institute of Machine Design, Cracow University of Technology*
*Al. Jana Pawła II 37, 31-864 Kraków, Poland*

(Received in the final form November 18, 2008)

Investigation of crack propagation can sometimes be a crucial stage of engineering analysis. The T-element method presented in this work is a convenient tool to deal with it. In general, T-elements are the Trefftz-type finite elements, which can model both continuous material and local cracks or inclusions. The authors propose a special T-element in a form of a pentagon with shape functions analytically modelling the vicinity of the crack tip. This relatively large finite element can be surrounded by even larger standard T-elements. This enables easy modification of the rough element grid while investigating the crack propagation. Numerical examples proved that the "moving pentagon" concept enables easy automatic generation of the T-element mesh, which facilitates observation of crack propagation even in very complicated structures with many possible crack initiators occurring for example in material fatigue phenomena.

## 1. Introduction

Fracture analysis of engineering structures often requires investigations of large variety of objects with different forms and positions of cracks. The crack propagation is often a key problem in practical engineering analysis. A path of the crack development can decide whether the final fracture causes damage of the whole structure or only eliminates its small part without total failure. Hence, such an analysis can influence a shape of a designed object. The main difficulty of this analysis is a large variety of possible development paths depending on a form and position of the initiation crack [1]. Therefore, it is important to possibly decrease the time of a single calculation in a searching loop. The T-element method is a convenient tool to deal with the problem. In general, T-elements are the Trefftz-type finite elements, in which internal shape functions fulfil governing differential equations of a certain boundary-value problem [23, 24]. They can model both continuous material and local cracks or inclusions.

Usually, the field near the crack tip is modelled with increased accuracy, which in case of the finite element method involves considerable remeshing in this area [9]. Recent investigations enable improvement of accuracy with minimal remeshing or field enrichment through a partition of unity methods [2, 10]. However, the most efficient way of proceeding seems to be in this case introduction of an analytical solution in the vicinity of the crack tip [4, 6, 11, 20]. It usually results in a hybrid-type finite element, because shape functions of the local solution do not conform with surrounding finite elements. The authors follow this path. They propose a special T-element in a form of a pentagon with shape functions analytically modelling the vicinity of the crack tip. This relatively large finite element can be surrounded by also large standard T-elements [5, 7, 8]. This enables easy modification of the rough element mesh while investigating the crack propagation.

The study includes detailed investigation of the T-element solution in comparison with the standard finite elements (ALGOR®, ANSYS®) [14]. Also, influence of geometry of an investigated object on stress intensity factors (SIF) and strain energy distribution has been studied. Finally, the interesting comparison of the crack propagation paths obtained by the standard finite element method and the hybrid Trefftz elements has been made [14].

Several numerical examples performed by the authors proved that the "moving pentagon" concept enables easy automatic generation of the T-element mesh, which facilitates observation of crack propagation even in very complicated structures with many possible crack initiators occurring for example in material fatigue phenomena.

## 2. T-COMPLETE SETS OF FUNCTIONS

A first step in formulation of any T-element is derivation of a complete system of functions (T-functions) identically fulfilling an equation of a considered problem. A review of such functions can be found in [7, 12, 25]. In case of an element with a V-notch (Fig. 1) T-complete systems are known as the Williams eigenfunctions [12, 22], which have the following form,

$$\sigma_{11} = \sum_n \mathrm{Re}\Big\{\lambda_n \rho^{\lambda_n - 1}\beta_n \left[(2 + \lambda_n \cos 2\alpha + \cos 2\lambda_n\alpha)\cos(\lambda_n - 1)\theta - (\lambda_n - 1)\cos(\lambda_n - 3)\theta\right] + \zeta_n \rho^{\zeta_n - 1}\eta_n \left[-(2 + \zeta_n \cos 2\alpha - \cos 2\zeta_n\alpha)\sin(\zeta_n - 1)\theta + (\zeta_n - 1)\sin(\zeta_n - 3)\theta\right]\Big\}, \quad (1)$$

$$\sigma_{22} = \sum_n \mathrm{Re}\Big\{\lambda_n \rho^{\lambda_n - 1}\beta_n \left[(2 - \lambda_n \cos 2\alpha - \cos 2\lambda_n\alpha)\cos(\lambda_n - 1)\theta + (\lambda_n - 1)\cos(\lambda_n - 3)\theta\right] + \zeta_n \rho^{\zeta_n - 1}\eta_n \left[(-2 + \zeta_n \cos 2\alpha - \cos 2\zeta_n\alpha)\sin(\zeta_n - 1)\theta - (\zeta_n - 1)\sin(\zeta_n - 3)\theta\right]\Big\}, \quad (2)$$

$$\sigma_{12} = \sum_n \mathrm{Re}\Big\{\lambda_n \rho^{\lambda_n - 1}\beta_n \left[-(\lambda_n \cos 2\alpha + \cos 2\lambda_n\alpha)\sin(\lambda_n - 1)\theta + (\lambda_n - 1)\sin(\lambda_n - 3)\theta\right] + \zeta_n \rho^{\zeta_n - 1}\eta_n \left[(\zeta_n \cos 2\alpha - \cos 2\zeta_n\alpha)\cos(\zeta_n - 1)\theta + (\zeta_n - 1)\cos(\zeta_n - 3)\theta\right]\Big\}, \quad (3)$$

$$\sigma_{33} = \begin{cases} 0 & \text{for plane stress state,} \\ \nu(\sigma_{11} + \sigma_{22}) = 4\nu \sum_n \mathrm{Re}\Big\{\lambda_n \rho^{\lambda_n - 1}\beta_n \cos(\lambda_n - 1)\theta - \zeta_n \rho^{\zeta_n - 1}\eta_n \sin(\zeta_n - 1)\theta\Big\} & \text{for plane strain state,} \end{cases} \quad (4)$$

where

$$\kappa = \begin{cases} \frac{3-\nu}{1+\nu} & \text{for plane stress state,} \\ 3 - 4\nu & \text{for plane strain state,} \end{cases} \quad (5)$$

$\rho = r/a$, $a$ is a scale parameter, $\beta_n$, $\eta_n$ are constants to be calculated from the element continuity conditions, and $\lambda_n$, $\zeta_n$ are the eigenvalues fulfilling the characteristic equations:

$$\sin 2\lambda_n\alpha + \lambda_n \sin 2\alpha = 0 \quad (6)$$

for the I kind of the notch (tension) and

$$\sin 2\zeta_n\alpha - \zeta_n \sin 2\alpha = 0 \quad (7)$$

for the II kind of the notch (in plane shear).

It should be underlined that in case of the T-elements the stress intensity factors can be obtained using only two constants for $n = 1$: $\beta_1$ and $\eta_1$. For $\alpha = \pi$ (crack) they have the form

$$K_I = \sqrt{2\pi a} \cdot \beta_1, \qquad K_{II} = -\sqrt{2\pi a} \cdot \eta_1. \quad (8)$$

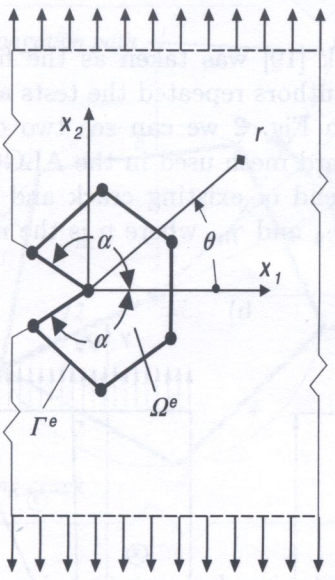


**Fig. 1.** Finite region containing special T-element with V notch; $\Omega^e$ – domain of element, $\Gamma^e$ – its boundary

## 3. HTD T-ELEMENT FORMULATION

In the HTD element standard relations between nodal forces $\mathbf{r}$ and nodal displacements $\mathbf{d}$ in the form $\mathbf{r} = \overset{\circ}{\mathbf{r}} + \mathbf{k}\mathbf{d}$, where $\mathbf{k}$ is a symmetric positive-definite stiffness matrix, are obtained from the condition [7, 8]

$$\int_{\Gamma^e} \delta\mathbf{t}^T(\mathbf{u} - \tilde{\mathbf{u}})\,\mathrm{d}\Gamma = \delta\mathbf{c}^T \int_{\Gamma^e} \mathbf{T}^T(\mathbf{u} - \tilde{\mathbf{u}})\,\mathrm{d}\Gamma = 0 \tag{9}$$

and the relation

$$\int_{\Gamma^e} \delta\tilde{\mathbf{u}}^T\mathbf{t}\,\mathrm{d}\Gamma = \int_{\Gamma_t^e} \delta\tilde{\mathbf{u}}^T\bar{\mathbf{t}}\,\mathrm{d}\Gamma + \delta\mathbf{d}^T\mathbf{r} \tag{10a}$$

or

$$\delta\mathbf{d}^T \int_{\Gamma^e} \tilde{\mathbf{N}}^T\mathbf{t}\,\mathrm{d}\Gamma = \delta\mathbf{d}^T \int_{\Gamma_t^e} \tilde{\mathbf{N}}^T\bar{\mathbf{t}}\,\mathrm{d}\Gamma + \delta\mathbf{d}^T\mathbf{r}, \tag{10b}$$

where the coefficient variation can be reduced.

The displacement vector $\mathbf{u}$ is expressed here by unknown coefficients $\mathbf{c}$ and a matrix $\mathbf{N}$ containing T-complete functions

$$\mathbf{u} = \overset{\circ}{\mathbf{u}} + \mathbf{N}\mathbf{c}, \qquad \mathbf{u} \in \Omega^e, \tag{11}$$

where $\overset{\circ}{\mathbf{u}}$ is a particular solution. Analogously we define tractions

$$\mathbf{t} = \overset{\circ}{\mathbf{t}} + \mathbf{T}\mathbf{c}, \qquad \mathbf{t} \in \Gamma^e \tag{12}$$

and the boundary frame function $\tilde{\mathbf{u}}$ has the form

$$\tilde{\mathbf{u}} = \tilde{\mathbf{N}}\mathbf{d}, \qquad \tilde{\mathbf{u}} = \Gamma^e, \tag{13}$$

where $\mathbf{d}$ are unknown frame coefficients (element degrees of freedom) and $\tilde{\mathbf{N}}$ is a polynomial matrix. If the element is situated near the object boundary $\Gamma_t^e$ along which the Neumann conditions are imposed, the tractions $\bar{\mathbf{t}}$ should be introduced as in Eq. (10).

The scale parameter $a$ in functions (1)–(4) allows to avoid numerical problems (real overflow or underflow). In the T-element modelling a crack it is usually taken as an average distance between an element mass centre and its nodes, Fig. 3.

## 4. Direction of crack propagation

An extended plate with a skew crack [19] was taken as the first numerical example. Following investigations presented in [6, 7] the authors repeated the tests and compared the results (stresses) with commercial programmes [14]. In Fig. 2 we can see two different FE meshes for the HTD formulation compared with the standard mesh used in the ALGOR® code. The next Fig. 3 shows the moving pentagon modelling the end of existing crack and indicating a new direction of the propagation path defined by angles $\theta_{Cn}$ and $\gamma_n$, where $n$ is the number of a calculation step.

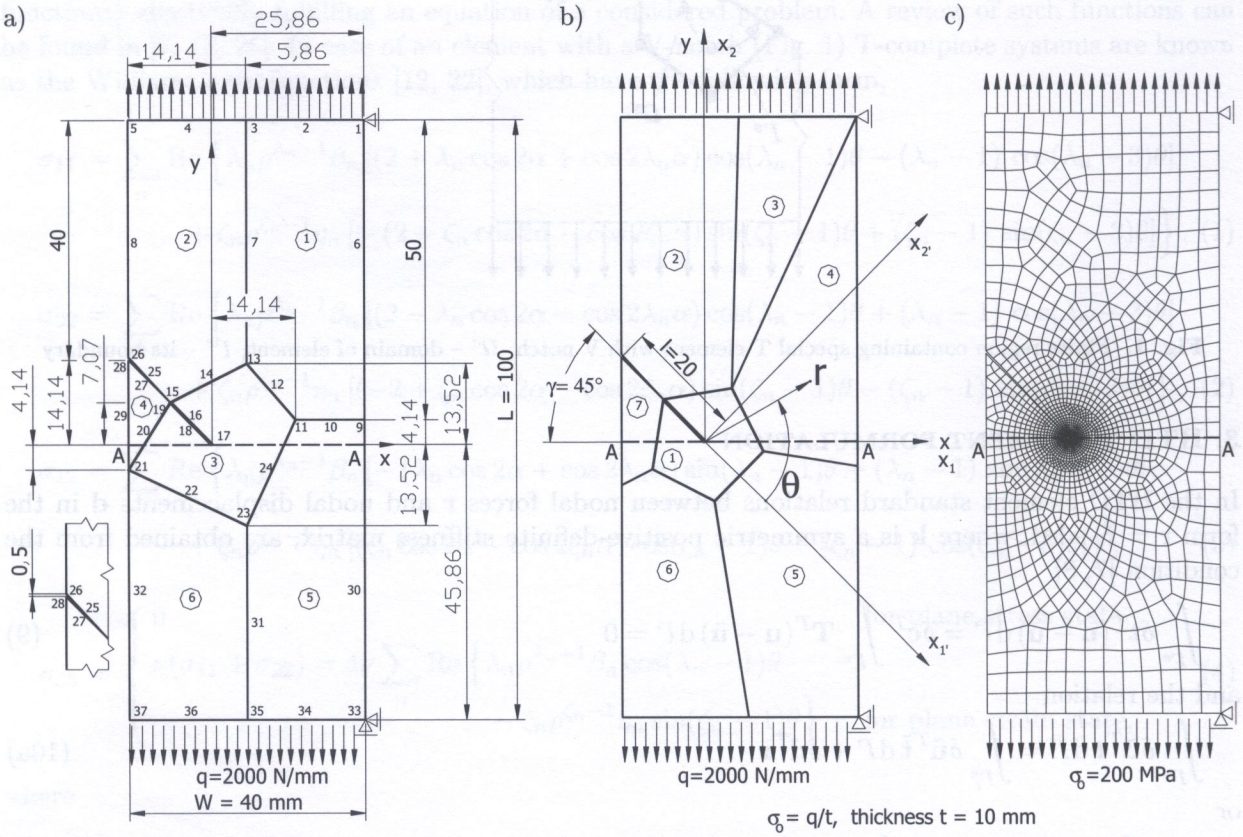


**Fig. 2.** Two different FE meshes for HTD formulation and coordinate system $(r, \theta)$ used for skew crack; a) irregular pentagon, b) regular pentagon, c) mesh obtained with ALGOR®

The following data were input to calculations: crack angle $\gamma = 315°$, length of the crack $l = 20\,\text{mm}$, overall dimensions $W \times L \times t = 40 \times 100 \times 10\,\text{mm}$, unit force $q = 2000\,\text{N/mm}$ uniformly loading the upper and lower edge of the plate, Poisson's ratio $\nu = 0.3$.

Stress intensity factors $K_I$ and $K_{II}$, Eq. (8), related to

$$K_0 = \sqrt{4\pi l}\,\sigma_0, \tag{14}$$

were calculated with the T-elements for the example defined in Fig. 2 ($K_0 = 100.3\,\text{MPa}\,\text{m}^{1/2}$). The results (presented in [13]) $K_I/K_0 = 0.6015$, $K_{II}/K_0 = -0.2911$, were in good agreement with values (0.6015 and −0.2910) published in [6, 7].

To determine direction in which a crack may grow, two classical hypotheses were taken into consideration. The first one was proposed by F. Erdogan and G.C. Sih [3] and is known as the maximum hoop stress criterion (MHSC). The hypothesis states that the crack extension starts at the crack tip and it grows in a radial direction indicated by the maximum tensile stress $\sigma_\theta$.

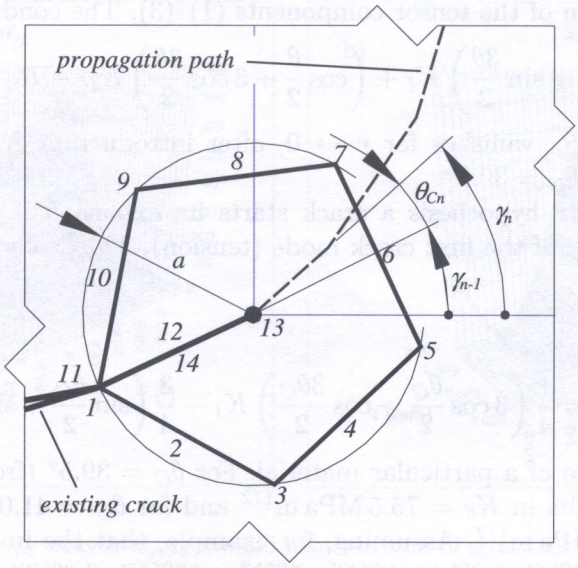


**Fig. 3.** Moving pentagon modelling end of existing crack and indicating new direction of propagation path defined by angles $\theta_{Cn}$, $\gamma_n$ ($n$ – number of current calculation step)

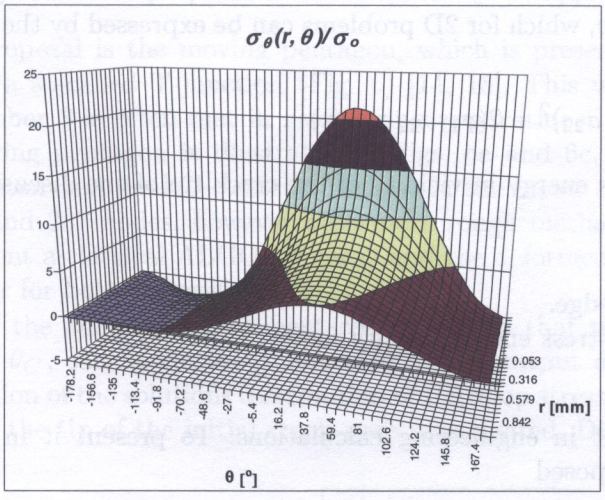


**Fig. 4.** Relative hoop stresses $\sigma_\theta/\sigma_0$ versus angle $\theta$ and radius $r$; crack propagates in direction of maximum of $\sigma_\theta$, i.e. for $\theta_C = 41°$

For the plate with the skew crack, Fig. 2, the distribution of $\sigma_\theta$ along circles $r$ = constant is presented in Fig. 4. The T-element solution with the transformation formula

$$\sigma_\theta = \frac{1}{2}\left[(\sigma_{11}+\sigma_{22}) - (\sigma_{11}-\sigma_{22})\cos 2(\theta+\gamma) - 2\sigma_{12}\sin 2(\theta+\gamma)\right], \tag{15}$$

where $\sigma_{ij}$, the stress output data of the system SAFE [6–8] is here applied. We observe a visible difference between this function and the other effort measures. The maximal value of $\sigma_\theta$, calculated for possibly small $r$, indicated direction of the crack propagation defined by the angle $\theta_C = 41.0°$.

A comparative solution with the use of the T-element code can be calculated from the formula

$$\sigma_\theta = \sum_{n=1}^{n_{\max}} \frac{n}{2}\rho^{\frac{n}{2}-1}\cdot\left\{\beta_n\left[\left(\frac{n}{2}+1\right)\cos\left(\frac{n}{2}-1\right)\theta - \left(\frac{n}{2}+(-1)^n\right)\cos\left(\frac{n}{2}+1\right)\theta\right]\right.$$
$$\left. + \eta_n\left[-\left(\frac{n}{2}+1\right)\sin\left(\frac{n}{2}-1\right)\theta + \left(\frac{n}{2}-(-1)^n\right)\sin\left(\frac{n}{2}+1\right)\theta\right]\right\} \tag{16}$$

obtained by transformation of the tensor components (1)–(3). The condition

$$\frac{\partial \sigma_\theta}{\partial \theta} = 0 \quad \rightarrow \quad \left(\sin\frac{\theta}{2} + \sin\frac{3\theta}{2}\right) K_I + \left(\cos\frac{\theta}{2} + 3\cos\frac{3\theta}{2}\right) K_{II} - R_n = 0, \tag{17}$$

where the residual term $R_n$ vanishes for $r \rightarrow 0$, after introduction $K_I = 0.6015 K_0$ and $K_{II} = 0.2910 K_0$ gives the result $\theta_C = 39.5°$.

According to the MHCS hypothesis a crack starts its extension if the maximum hoop stress reaches a critical value $\sigma_{IC}$ of the first crack mode (tension). This leads to the condition

$$K_\theta \geq K_{IC}\,, \tag{18}$$

where

$$K_\theta = \lim_{r\to 0} \sqrt{2\pi r}\, \sigma_{\theta\,\max} = \frac{1}{4}\left(3\cos\frac{\theta_C}{2} + \cos\frac{3\theta_C}{2}\right) K_I - \frac{3}{4}\left(\sin\frac{\theta_C}{2} + \sin\frac{3\theta_C}{2}\right) K_{II}\,, \tag{19}$$

$K_{IC}$ is the crack resistance of a particular material. For $\theta_C = 39.5°$ (from Eq. (17)) the left-hand side of that equation results in $K_\theta = 76.5\,\mathrm{MPa\,m^{1/2}}$ and for $\theta_C = 41.0°$ (direct calculations with SAFE) gives $K_\theta = 77.2\,\mathrm{MPa\,m^{1/2}}$. Assuming, for example, that the investigated plate is made of tempered alloy steel (0.03%C, 0.2%Al, 8%Co, 5%Mo, 18%Ni, 0.6%Ti, $K_{IC} = 78\,\mathrm{MPa\,m^{1/2}}$) the tension $\sigma_0 = 200\,\mathrm{MPa}$ will not initiate the crack propagation in the plate. However, because of the very small differences between $K_\theta$ and $K_{IC}$ we should consider this state as not admissible.

The second hypothesis applied by the authors was first proposed also by Sih [16–18] and is based on strain energy density $w$, which for 2D problems can be expressed by the stress tensor components as

$$w = \frac{1}{4G}\left[\frac{\kappa+1}{4}(\sigma_{11}+\sigma_{22})^2 - 2(\sigma_{11}\sigma_{22} - \sigma_{12}^2)\right]. \tag{20}$$

Figure 5a presents this energy in vicinity of the crack tip of the discussed plate as related to

$$w_q = \frac{1}{G}\cdot\frac{\kappa+1}{16}\cdot\sigma_0^2 \tag{21}$$

calculated for its loaded edge.

Sih introduced also a stress energy-density factor $S$

$$S = wr, \tag{22}$$

which is more convenient in engineering calculations. To present it in a non-dimensional form (Fig. 5b) the authors proposed

$$S_q = w_q r_q\,, \tag{23}$$

where $r_q$ is the smallest distance from the crack tip to the loaded edge of the plate. This second Sih's hypothesis postulates that the crack extends from its tip in the radial direction defined by a local minimum of the stress energy-density factor $S$. This minimum should be situated between two local maxima in front of a line normal to the crack tip [21], i.e. $[-90°, +90°]$, Fig. 5. Using that criterion and the results obtained with the T-element code, the value $\theta_C = 36.6°$ defining direction of the crack propagation was obtained.

Following considerations presented above (compare Eq. (17)), which lead to

$$[\sin 2\theta - (\kappa-1)\sin\theta]\, K_I^2 - 2[(\kappa-1)\cos\theta - 2\cos 2\theta]\, K_I K_{II} + [(\kappa-1)\sin\theta - 3\sin 2\theta]\, K_{II}^2 = 0 \tag{24}$$

after numerical solution of that equation the value $\theta_C = 35.04°$ was determined. A condition of crack propagation for the strain energy-density hypothesis [18] can be written as

$$S_{\min} \geq S_C(K_{IC}\,, K_{IIC}). \tag{25}$$

The critical value $S_C$ depends here on both $K_{IC}$ and $K_{IIC}$, which is less convenient, because the shear crack resistance is in many cases unavailable.

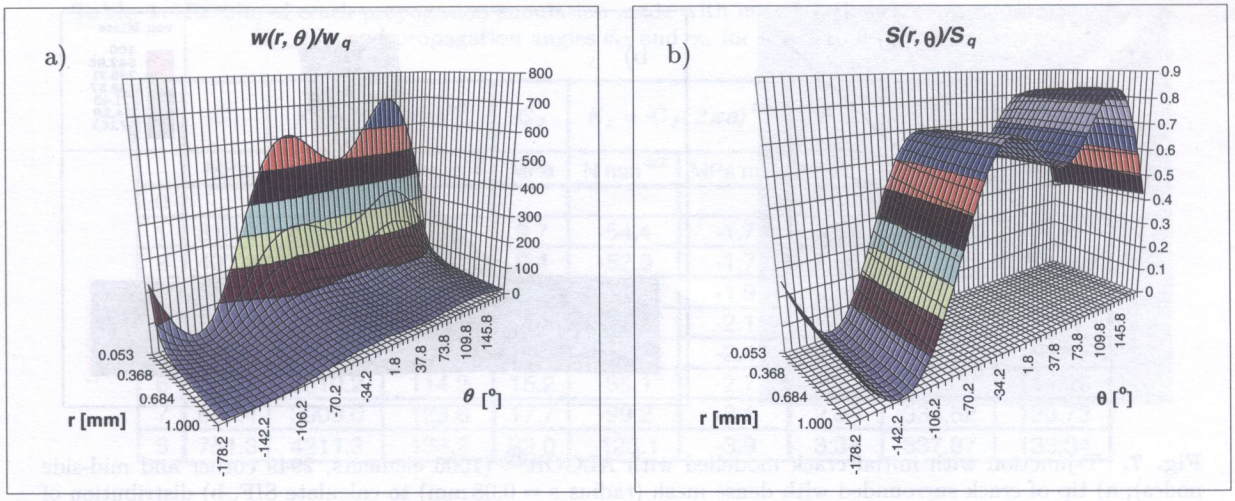


**Fig. 5.** Relative strain energy density $w/w_q$ (a) and relative factor of strain energy density $S/S_q$ around tip of crack (b)

## 5. Prediction of crack propagation path

The basic idea of the proposal is the moving pentagon, which is presented below in an example of crack propagation in a so-called T-junction (Fig. 6) [14, 15]. This welded joint of two sheets 1, 2 reinforced by a member 3 is often met in engineering applications, e.g. in frames of vehicles. The concept of the moving pentagon is illustrated in Figs. 6a and 6c, in which we can observe automatically defined initial and final T-element meshes. In the latter case the SAFE model was built with 82 elements and 281 nodes, however even more rough meshes gave acceptable results. For comparison, we present a classical ALGOR® mesh and the deformed model — Fig. 7 with the stress distribution similar for both FE systems.

One of advantages of the analytical T-element code is a fact that the stress intensity factors $K_I$, $K_{II}$, and the angle $\theta_C$, can be explicitly obtained as the output data of the system SAFE. Nevertheless, for verification of the solutions distribution of the hoop stress $\sigma_\theta$ and the factor of strain energy-density $S$ around the tip of the initial crack were investigated. Diagrams of both quantities

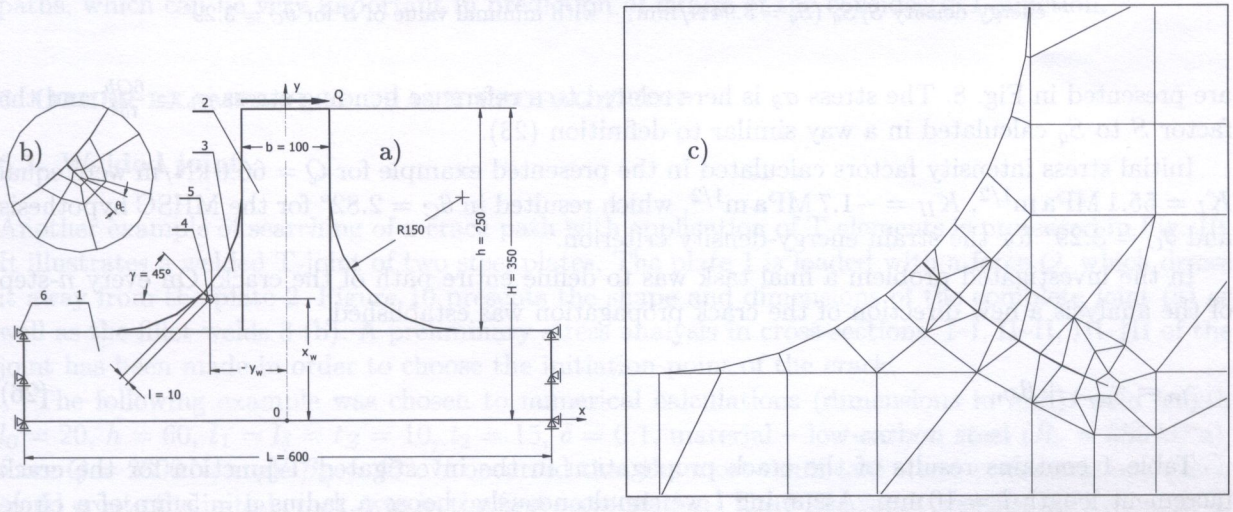


**Fig. 6.** T-junction of plates 1, 2 with fillet member 3; a) load $Q$, boundary constraints and dimensions (mm): crack 4 of length $l = 10$ mm, thickness $t = 10$ mm, initial angle $\gamma = 315°$; T-element (moving pentagon) around tip of crack noted as 5, b) definition of angle $\theta_C$, c) propagation path after 8 steps

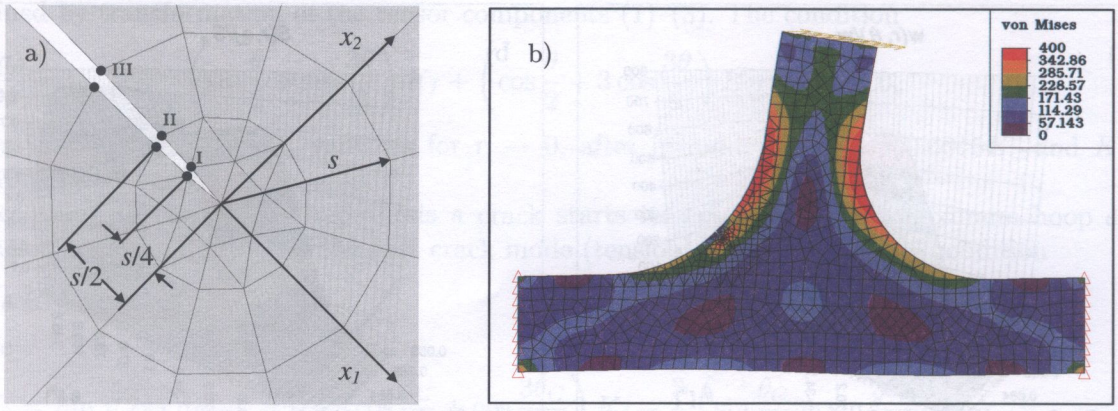


**Fig. 7.** T-junction with initial crack modelled with ALGOR® (1006 elements, 2949 corner and mid-side nodes); a) tip of crack surrounded with dense mesh (radius $s = 0.08\,\text{mm}$) to calculate SIF, b) distribution of von Mises equivalent stresses $\sigma_{vM}$ (displaced model with scale = 20)

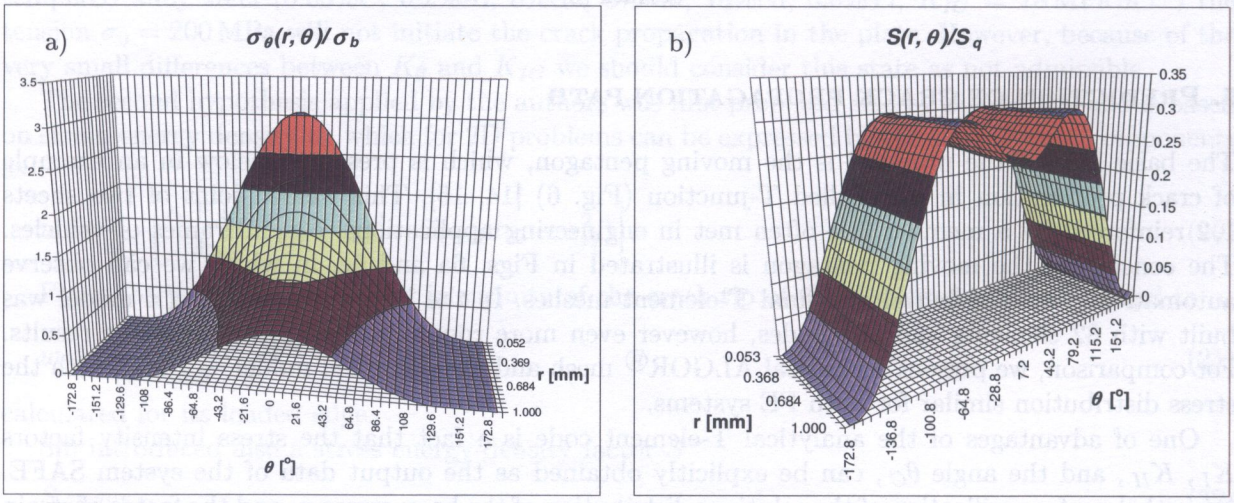


**Fig. 8.** T-element results around crack tip - curves concern circles $r = 0.053 \div 1\,\text{mm}$; a) diagram of relative hoop stress $\sigma_\theta/\sigma_b$ ($\sigma_b = 1000\,\text{MPa}$) with maximum for $\theta_C = 2.82°$ and b) diagram of relative factor of strain energy density $S/S_q$ ($S_q = 5.94\,\text{N/mm}$) – with minimal value of $S$ for $\theta_C = 3.29°$

are presented in Fig. 8. The stress $\sigma_\theta$ is here related to a reference bending stress $\sigma_b = \frac{6Qh}{tb^2}$ and the factor $S$ to $S_q$ calculated in a way similar to definition (23).

Initial stress intensity factors calculated in the presented example for $Q = 66.6\,\text{kN/m}$ were equal $K_I = 55.1\,\text{MPa}\,\text{m}^{1/2}$, $K_{II} = -1.7\,\text{MPa}\,\text{m}^{1/2}$, which resulted in $\theta_C = 2.82°$ for the MHSC hypothesis and $\theta_C = 3.29°$ for the strain energy-density criterion.

In the investigated problem a final task was to define entire path of the crack. On every $n$-step of the analysis a new direction of the crack propagation was established,

$$\gamma_n = \gamma_{n-1} + \theta_{Cn}\,. \tag{26}$$

Table 1 contains results of the crack propagation in the investigated T-junction for the crack increment length $l = 10\,\text{mm}$. Assuming $l$ we simultaneously choose a radius $a = 5\,\text{mm}$ of a circle circumscribing the leading pentagon. To check influence of the user-defined increment $l$ on shape of the path, the calculations were repeated for $a = 2.5\,\text{mm}$. Figure 9a presents both paths. It is clearly seen that on this level of the increment length its influence is rather small.

**Table 1.** Results of crack propagation simulation made with use of T-elements: stress intensity factors $K_I$, $K_{II}$ and propagation angles $\theta_C$ and $\gamma_n$ for $n = 1$ to 8 ($a = 5$ mm)

| $n$ | $C_1$ | $K_I = C_1(2\pi a)^{1/2}$ | | $C_2$ | $K_{II} = -C_2(2\pi a)^{1/2}$ | | $\theta_{Cn}$ | $\gamma_n = \gamma_{n-1} + \theta_{Cn}$ | $K_\theta$ |
|---|---|---|---|---|---|---|---|---|---|
| | MPa | N mm$^{-3/2}$ | MPa m$^{1/2}$ | MPa | N mm$^{-3/2}$ | MPa m$^{1/2}$ | ° | ° | MPa m$^{1/2}$ |
| 0 | | | | | | | 0 | 315 | |
| 1 | 310.9 | 1742.6 | 55.1 | 9.7 | -54.4 | -1.7 | 3.57 | 318.57 | 55.19 |
| 2 | 407.8 | 2285.7 | 72.3 | 9.4 | -52.9 | -1.7 | 2.65 | 321.22 | 72.34 |
| 3 | 477.3 | 2675.3 | 84.6 | 10.8 | -60.5 | -1.9 | 2.59 | 323.81 | 84.67 |
| 4 | 536.6 | 3007.4 | 95.1 | 11.8 | -66.1 | -2.1 | 2.51 | 326.32 | 95.17 |
| 5 | 591.2 | 3313.8 | 104.8 | 13.4 | -75.3 | -2.4 | 2.60 | 328.92 | 104.87 |
| 6 | 644.1 | 3610.2 | 114.2 | 15.2 | -85.1 | -2.7 | 2.70 | 331.62 | 114.26 |
| 7 | 697.4 | 3909.0 | 123.6 | 17.7 | -99.2 | -3.1 | 2.90 | 334.52 | 123.73 |
| 8 | 751.3 | 4211.3 | 133.2 | 22.0 | -123.1 | -3.9 | 3.34 | 337.87 | 133.34 |

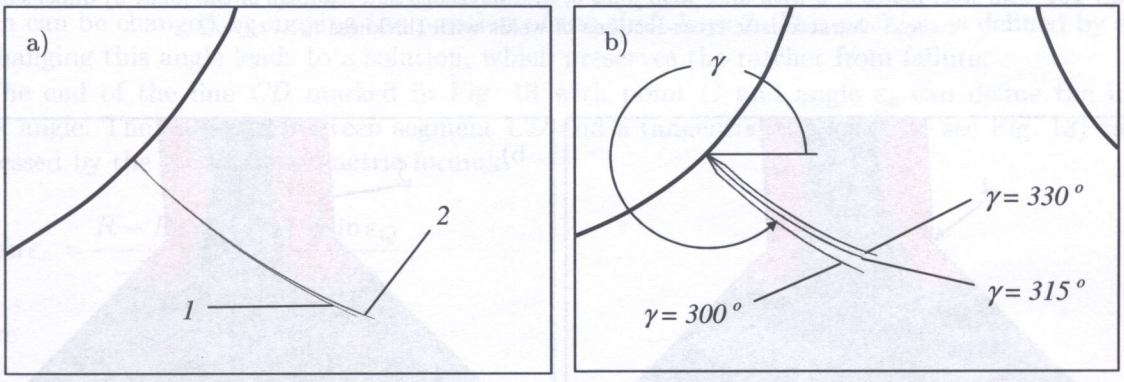


**Fig. 9.** Crack propagation path in T-junction obtained with T-elements (similarity of notations accidental); a) paths of crack built: 1 – with pentagon of $a = 5$ mm and 2 – with pentagon of $a = 2.5$ mm, b) paths of crack with different initial angles $\gamma$: 300°, 315°, 330°

A more significant effect observed in the investigated phenomenon is shown in Fig. 9b. We can observe that even considerably different initial crack angles result in nearly parallel propagation paths, which can be very important in prediction of failure of the considered T-junction.

## 6. Other examples of crack propagation

### 6.1. Welded joint

Another example of searching of a crack path with application of T-elements is presented in Fig. 10. It illustrates a welded T-joint of two steel plates. The plate 1 is loaded with a force $Q$, which draws it away from the plate 2. Figure 10 presents the shape and dimensions of the complete joint (a) as well as the fillet welds 3 (b). A preliminary stress analysis in cross-sections: I–I, II–II, III–III of the joint has been made in order to choose the initiation point of the crack.

The following example was chosen to numerical calculations (dimensions in mm): weld length $l_0 = 20$, $h = 60$, $t_1 = l_\delta = t_Z = 10$, $t_2 = 15$, $\delta = 0.1$, material – low-carbon steel ($R_e = 355$ MPa), force $Q = 2800$ N, angle $\beta_Q = 45°$. It occurred that the most significant stress concentration, which could create the initial crack, was in the first cross-section. The FEM result was 504 MPa in point 4, Fig. 11a, which obviously refers to section I–I. Similar analysis was done for the model with the initial crack – point 5 in Fig. 11b – where the von Mises equivalent stress $\sigma_{vM}$ achieved (for a similar mesh) value 585 MPa.

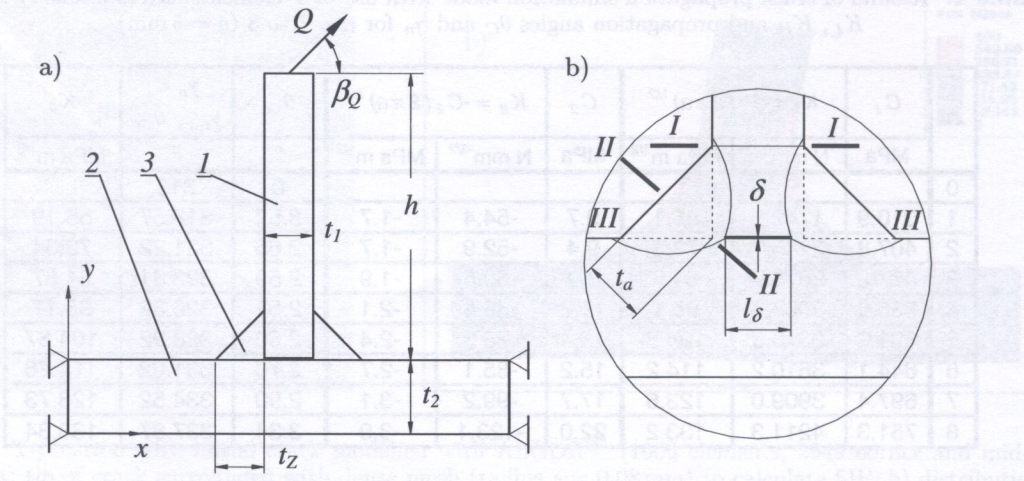


**Fig. 10.** Two steel plates 1, 2 with fillet weld joint 3; a) dimensions and loadings of the joint, b) dimensions and characteristic cross-sections of welds with thickness $t_a = t_Z/\sqrt{2}$

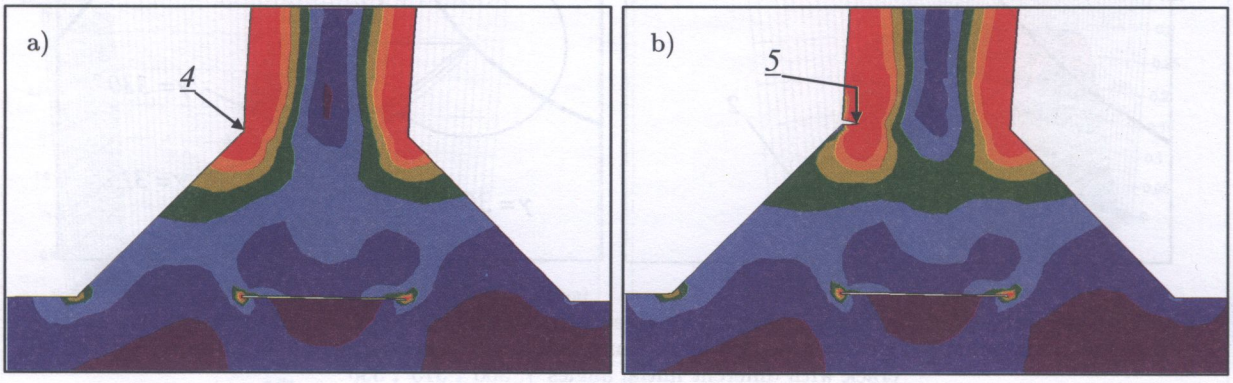


**Fig. 11.** Von Mises equivalent stress ($\sigma_{vM}$) distribution in region of welded joint; figures present deformed models (scale = 20); a) joint without crack — concentration at point 4, b) model with initial crack — concentration at point 5

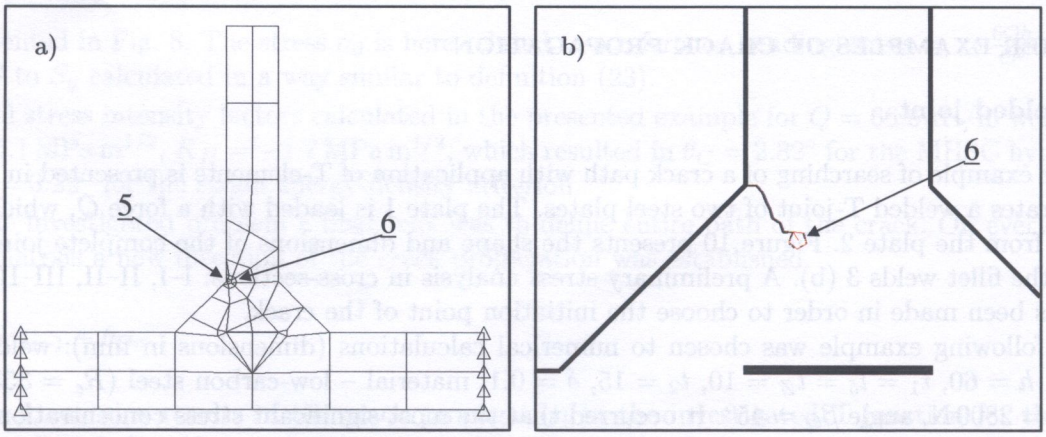


**Fig. 12.** Model of welded joint with T-elements including moving pentagon 6 ($a$ = 0.5 mm); a) mesh in a starting phase of simulation (with notch 5), b) fragment with crack path plotted after some steps of calculations

Figure 12 presents a model of the welded joint, which uses the T-elements including the moving pentagon 6. In Fig. 12a we observe mesh of the Trefftz FEA model in a starting phase (with initial crack 5) of the simulation, whereas Fig. 12b presents a fragment of the joint with a crack path plotted after several steps of the calculations. The T-element mesh uses the regular pentagon with the radius $a = 0.5\,\text{mm}$ (see Fig. 3). Application of such a small element was caused by the mesh configuration near the very narrow gap ($\delta = 0.1\,\text{mm}$) under the vertical joint member (see Fig. 10b). However, this inconvenience may be eliminated by introduction of other two pentagons containing the ends of the inter-member gap.

### 6.2. Crack propagation in a ratchet-wheel

In Fig. 13 shape, dimensions and loads of the ratchet-wheel 1 and other coworking elements are defined. Torque of shaft 3 is introduced by a pusher. One tooth of the ratchet-wheel is loaded by the pusher with force $Q$, which — mainly through the keys 2 — is then transmitted to the shaft 3.

The ratchet-wheel 1 has a possible failure path along cross-section $CD$, width and position of which can be changed by moving the position of the shaft keys 2. This position is defined by angle $\varepsilon$. Changing this angle leads to a solution, which preserves the ratchet from failure.

The end of the line $CD$ marked in Fig. 13 with point $C$ and angle $\varepsilon_c$ can define the initial crack angle. The angle $\varepsilon_c$ (between segment $CD$ and a tangential to circle $R$ – see Fig. 13) can be expressed by the following geometric formula

$$\tan\varepsilon_c = \frac{R - H_2\cos\varepsilon_Q - \frac{b}{2}\sin\varepsilon_Q}{-H_2\sin\varepsilon_Q + \frac{b}{2}\cos\varepsilon_Q}, \tag{27}$$

where

$$\varepsilon_Q = \frac{\pi}{2z} - \varepsilon, \qquad z \text{ – number of teeth,} \tag{28}$$

and may be used to set the initial crack angle $\gamma$.

Figure 14 presents the T-element meshes with the moving pentagon 5 used for crack propagation in the ratchet-wheel. The object was clamped in nodes 6. Two different initial notches 5, one near the tooth corner $C$ and the other at the keyway corner, were used for searching the crack path.

Position of the key against the tooth, which is loaded with the force $Q$, can be changed with the angle $\varepsilon$. This may lead to certain optimal solution decreasing probability of failure. Full optimisation of this structure is not the aim of this paper, however, results presented here may be used as outlines for a designer.

Figure 15 presents results obtained by simulation of the crack propagation for two cases (a) and (b) defined in Fig. 14. Position of the key against the tooth loaded with the force $Q$ was assumed in such a way that (ref. to Fig. 13) the angle $\varepsilon_c = 90°$, the angle $\varepsilon_Q = 13.57°$ and the angle $\varepsilon = 1.43°$. Remaining data were as follows (dimensions in mm): $z = 6$, $d = 50$, key height $h = 9$, key width $b = 14$, $s = 4.5$, key length $l_0 = 10$, $R = 41.6$, $H_1 = 19.5$, $H_2 = 29$, tooth height $h_t = 8$, $h_Q = 6$, $Q = 17.46\,\text{kN}$. Initial crack direction refers to angle $\varepsilon_c = 90°$ and gives the values: $\gamma = 120°$ for case (a) and $\gamma = 300°$ for case (b) (Figs. 14, 15).

In case of starting point $C$ (Fig. 15a) the end of the crack path cuts the bottom surface of the keyway, which causes failure of the rim of the ratchet-wheel. In the second case (Fig. 15b) the end of the crack path crosscuts the side surface of the tooth, which also leads to failure.

Another set of results obtained by simulation of the crack path in the ratchet-wheel is presented in Fig. 16. They concern the wheel with a shifted keyway (angle $\varepsilon = -13.57°$). Calculations were made with use of the T-elements including the moving pentagon ($a = 1\,\text{mm}$) with the initial crack positioned near the corner of the tooth root. Four cases of the angle $\gamma$ were investigated: a) 120°, b) 150°, c) 180° and d) 210°.

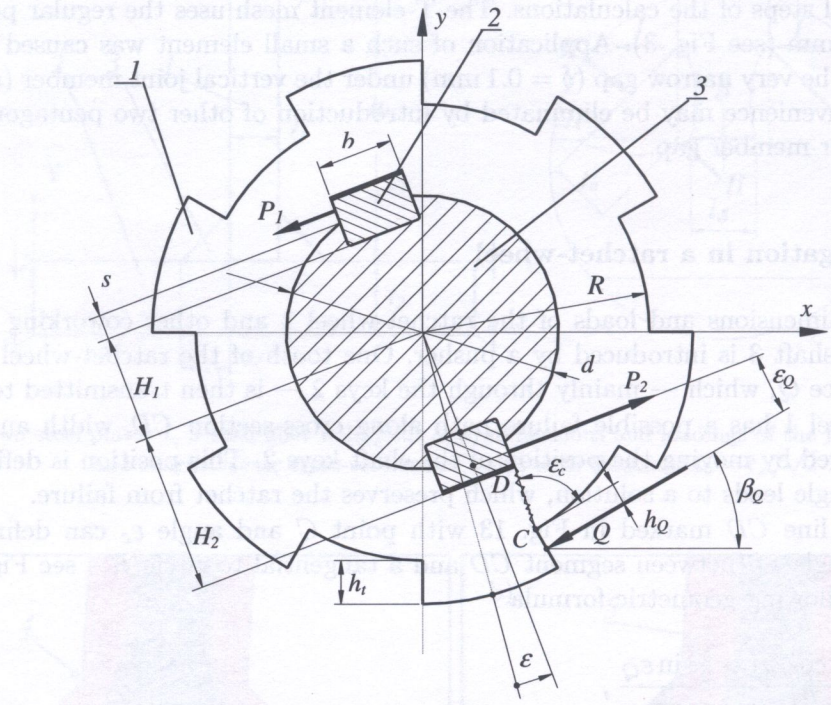


**Fig. 13.** Geometry and loading of ratchet-wheel 1 and other elements: keys 2, shaft 3; $CD$ – possible failure cross-section, $\varepsilon$ – angle defining position of key

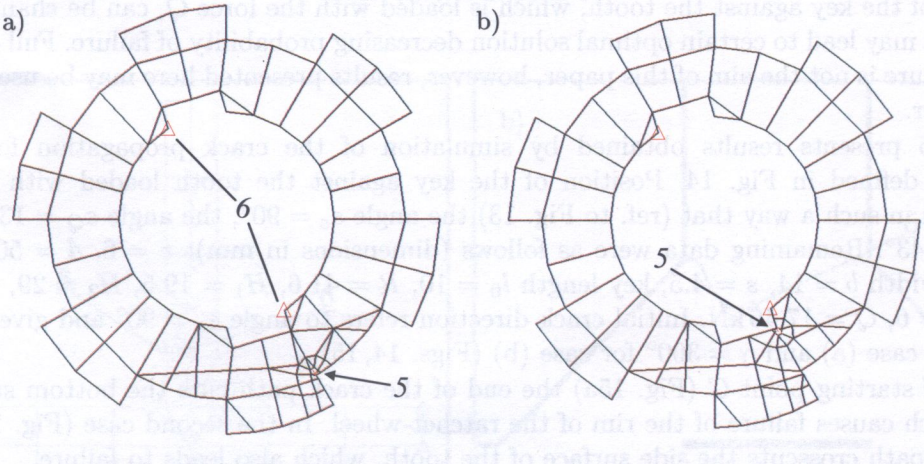


**Fig. 14.** T-element mesh for crack propagation in ratchet-wheel with boundary constraints 6; two different initial notches 5 for searching path of crack: a) at tooth root corner, b) at keyway corner

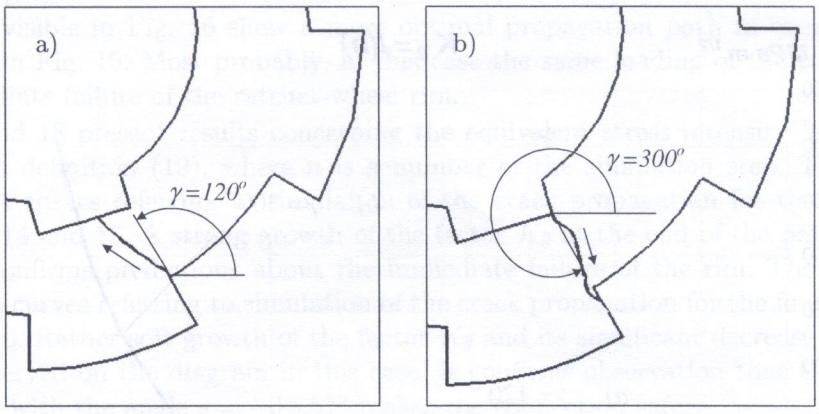


**Fig. 15.** Crack paths in ratchet-wheel ($\varepsilon = 1.43°$) defined with use of T-elements including moving pentagon ($a = 1\,\text{mm}$) with initial crack a) at tooth root corner, b) at keyway corner

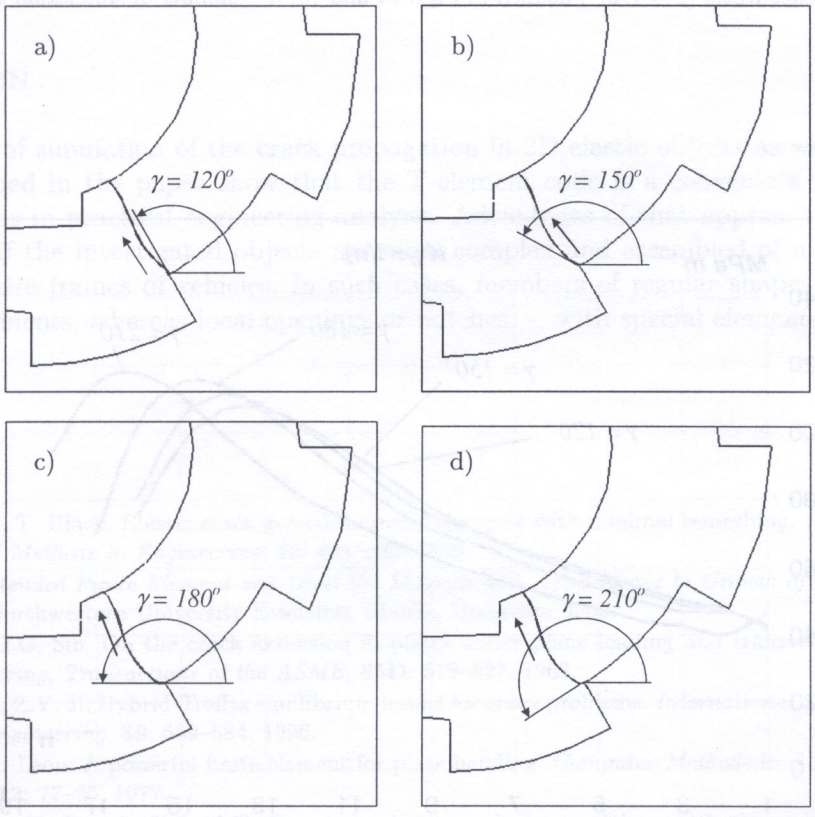


**Fig. 16.** Crack paths in ratchet-wheel with shifted keyway ($\varepsilon = -13.57°$) determined with T-elements including moving pentagon ($a = 1\,\text{mm}$); initial crack angle $\gamma$: a) 120°, b) 150°, c) 180°, d) 210°

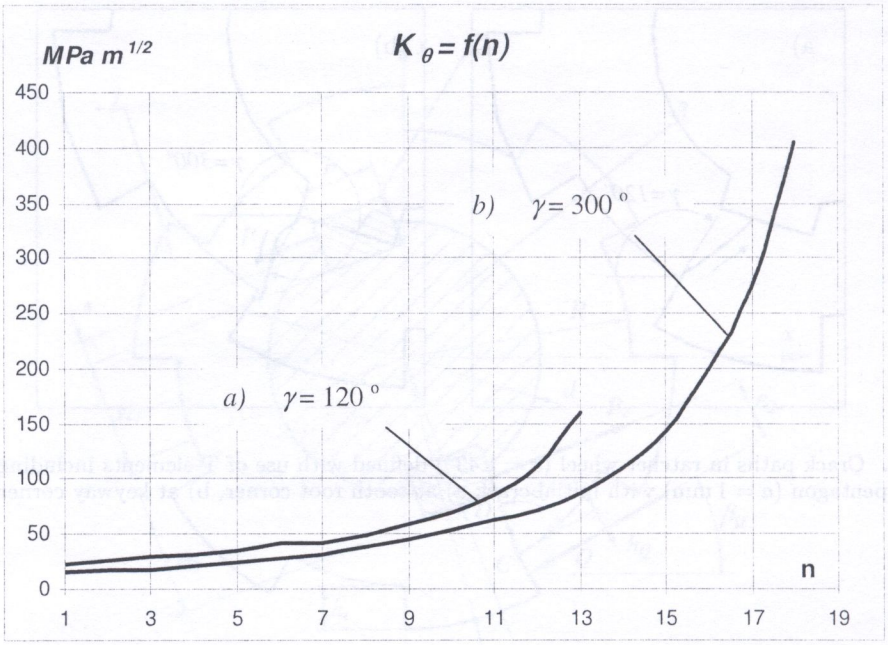


**Fig. 17.** Equivalent stress intensity factor $K_\theta = f(n)$ for two cases (a, b) of simulation of crack path in ratchet-wheel ($\varepsilon = 1.43°$) defined in Figs. 14 and 15; $n$ – number of simulation step

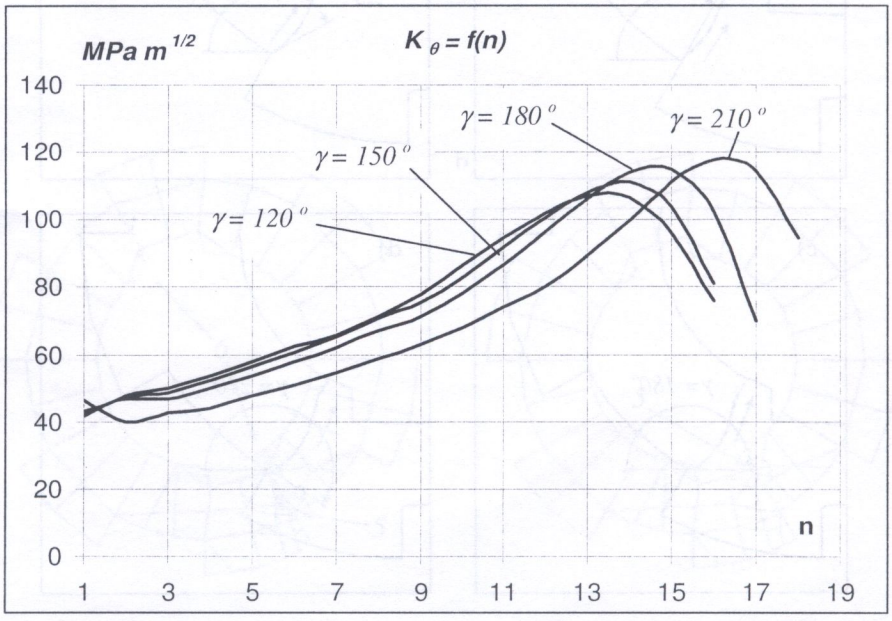


**Fig. 18.** Equivalent stress intensity factor $K_\theta = f(n)$ for four cases of crack path simulation in ratchet-wheel defined in Fig. 16 ($\varepsilon = -13.57°$); $n$ –number of simulation step

A changed position of the key against the loaded tooth — $\varepsilon = -13.57°$ instead of $1.43°$ — was applied in order to avoid a rapid failure of the wheel. The remaining data (load and dimensions) were left unchanged.

Crack paths visible in Fig. 16 show a more optimal propagation path in comparison with the cases presented in Fig. 15. Most probably, in this case the same loading of the tooth side will not make the immediate failure of the ratchet-wheel rim.

Figures 17 and 18 present results concerning the equivalent stress intensity factor $K_\theta = f(n)$, according to the definition (19), where $n$ is a number of the simulation step. The first diagram, Fig. 17, contains curves referring to simulation of the crack propagation for the two cases (a, b) defined in Figs. 14 and 15. A strong growth of the factor $K_\theta$ at the end of the path — particularly in case (b) — confirms predictions about the immediate failure of the rim. The second diagram, Fig. 18, contains curves referring to simulation of the crack propagation for the four cases (a, b, c, d) defined in Fig. 16. Rather soft growth of the factor $K_\theta$ and its significant decrease at the end of the path can be observed on the diagram in this case. It confirms observation that the rotation of the keyway position with the angle $\varepsilon = -13.57°$ makes the connection safer.

The growth of the function $K_\theta(n)$ observed in Fig. 17 is caused by the force $P_2$ (Fig. 15a) or by the force $Q$ (Fig. 15b) and by the remaining cross-section of the rim decreasing during the path propagation. It makes the strong tensile hoop stress near the tip of the crack, hence, the factor $K_\theta$ grows. Different situation takes place in Fig. 18, where the decrease of the function $K_\theta(n)$ at the end of the path is observed in every of the four cases. In this case (Fig. 16), forces $Q$ and $P_2$ always act on the same side of the crack path. A special effect is made by the force $P_2$, which compresses the remaining, decreasing cross-section of the rim. It makes smaller the tensile hoop stress near the tip of the crack and diminishes the function $K_\theta(n)$.

## 7. Conclusion

The procedures of simulation of the crack propagation in 2D elastic objects as well as other investigations described in the paper show that the T-element code is a convenient tool to deal with fracture problems in practical engineering analysis. Advantages of that approach can appear even more evidently if the investigated objects are more complex and assembled of numerous parts as, for example, entire frames of vehicles. In such cases, members of regular shapes can be modelled with large T-elements, whereas local openings or notches — with special elements presented in the paper.

## References

[1] T. Belytschko, T. Black. Elastic crack growth in finite elements with minimal remeshing. *International Journal for Numerical Methods in Engineering*, **45**: 601–620, 1999.

[2] S. Bordas. *Extended Finite Element and Level Set Methods with Applications to Growth of Cracks and Biofilms.* PhD thesis, Northwestern University Evanston, Illinois, December 2003.

[3] F. Erdogan, G.C. Sih. On the crack extension in plates under plane loading and transverse shear. *Journal of Basic Engineering, Transactions of the ASME*, **85D**: 519–527, 1963.

[4] J.A.T. Freitas, Z.Y. Ji. Hybrid-Trefftz equilibrium model for crack problems. *International Journal for Numerical Methods in Engineering*, **39**: 569–584, 1996.

[5] J. Jirousek, N. Leon. A powerful finite element for plate bending. *Computer Methods in Applied Mechanics and Engineering*, **12**: 77–96, 1977.

[6] J. Jirousek, A. Venkatesh. Hybrid-Trefftz plane elasticity elements with p-method capabilities. *International Journal for Numerical Methods in Engineering*, **35**: 1443–1472, 1992.

[7] J. Jirousek, A. Wróblewski. T-elements: State of the art and future trends. *Archives of Computational Methods in Engineering*, **3/4**: 323–434, 1996.

[8] J. Jirousek, A.P. Zieliński. Survey of Trefftz-type element formulations. *Computers and Structures*, **63**(2): 225–242, 1997.

[9] D.G. Lewicki, R. Ballarini. *Effect of rim thickness on gear crack propagation path.* NASA Technical Memorandum 107229, Army Research Laboratory Technical Report ARL-TR-1110. Prepared for the *7th International Power Transmission and Gearing Conference*, October 6–9, 1996, sponsored by the ASME, San Diego, California. Available: http://gltrs.grc.nasa.gov/reports/1996/TM-107229.pdf.

[10] N. Moës, J. Dolbow, T. Belytschko. A Finite element method for crack growth without remeshing. *International Journal for Numerical Methods in Engineering*, **46**: 131–150, 1999.

[11] R. Piltner. Special finite elements with holes and internal cracks. *International Journal for Numerical Methods in Engineering*, **21**: 1471–1485, 1985.

[12] Q.H. Qin. *The Trefftz Finite and Boundary Element Method*, WITpress, Southampton, 2000.

[13] H. Sanecki, A.P. Zieliński, S. Łaczek. *Application of Analytical Finite Elements to Crack Problems* (in Polish), Grant T11F 012 23 of KBN (Polish State Committee for Scientific Research), Report, Part I, Cracow, 2003.

[14] H. Sanecki, A.P. Zieliński. Crack propagation modelled by T-elements. *Engineering Computations.* **23**(2): 100–123, 2006.

[15] H. Sanecki, A.P. Zieliński. Application of T-elements to crack path prediction in 2D engineering structures. *CMM2005* Częstochowa 21–24 June 2005, pp. 27. ISBN 83-921605-7-6/CD.

[16] G.C. Sih. Energy-density concept in fracture mechanics. *Engineering Fracture Mechanics*, **5**: 1037–1040, 1973.

[17] G.C. Sih. Some basic problems in fracture mechanics and new concepts. *Engineering Fracture Mechanics*, **5**: 365–377, 1973.

[18] G.C. Sih. Strain energy-density factor applied to mixed-mode crack problems. *International Journal of Fracture*, **10**: 305–321, 1974.

[19] B.A. Szabo, J. Babuška. *Computation of the Amplitude of Stress Singular Terms for Cracks and Reentrant Corners.* Report WU/CCM-86/1, Washington Univ. In St. Louis, February 1986.

[20] P. Tong, P.H. Pian, S.L. Lasry. A hybrid-element approach to crack problems in plane elasticity. *International Journal for Numerical Methods in Engineering*, **7**: 297–308, 1973.

[21] G. N. Wells. *Discontinuous Modelling of Strain Localisation and Failure.* PhD thesis (Proefschrift ter verkrijging van de graad van doctor aan de Technische Universiteit Delft), 2001.

[22] M.L. Williams. Stress singularities resulting from various boundary conditions in angular corners of plates in extension. *Journal of Applied Mechanics*, **19**: 526–528, 1952.

[23] A.P. Zieliński, O.C. Zienkiewicz. Generalized finite element analysis with T-complete boundary solution functions. *International Journal for Numerical Methods in Engineering*, **21**: 509–528, 1985.

[24] A.P. Zieliński, I. Herrera. Trefftz method: fitting boundary conditions. *International Journal for Numerical Methods in Engineering*, **24**: 871–891, 1987.

[25] A.P. Zieliński. On trial functions applied in the generalized Trefftz method. *Advances in Engineering Software*, **24**: 147–155, 1995.